

Resolution for creating optical potentials

Max N. Frankel

max.frankel@stonybrook.edu

Department of Physics and Astronomy,
Stony Brook University

August 17, 2022

Contents

1 Motivation	2
2 Microscope objective for looking at tiny images	2
3 Fiber mode field diameter measurements	3
3.1 Using the microscope objective to directly measure waist	3
3.2 Calculation of waist from beam divergence angle	4
3.2.1 Razor blade technique for measuring beam radius	6
4 Choosing a focusing lens	9
5 Choosing a collimating lens	11
6 Telescope for beam expansion	14
7 Imaging an edge	15
7.1 Single lens	16
7.2 Two lenses	18
7.2.1 Setup	18
7.2.2 Results	19
7.2.3 Beam size	20
7.2.4 Image demagnification	22
8 Conclusions	24

1 Motivation

The goal of this project was to create an optical system that could project arbitrary intensity distributions of light onto a Bose-Einstein Condensate. A 790nm diode laser producing a lowest-order Gaussian beam was chosen as a light source. To shape the beam into an arbitrary distribution, it was decided to use an amplitude mask, which simply blocks parts of the beam passing through the mask.

The simplest amplitude mask is any sharp edge, such as a razor blade, that can be used to block a section of the beam. In this report, a 1951 USAF resolution target was used as an amplitude mask. Eventually, we hope to use a DMD as an amplitude mask, as arbitrary patterns can be easily designed and displayed.

In direct imaging, a single lens is used to focus the light produced by an object into an image. We would like to have the amplitude mask as the object. By translating the lens, the location of the focused image can be adjusted. This simple system was chosen for projecting an image onto a Bose-Einstein condensate.

The Bose-Einstein condensates formed in Professor Schneble's lab are about $10\mu\text{m}$ in diameter, and are loaded into a lattice with a spacing of about 340nm . Thus, we need to create images that have features on the order of single microns, and we must devise a way to look at these images, to verify that we are creating them.

2 Microscope objective for looking at tiny images

To observe and record the images created, a $50\times$ Mitutoyo microscope objective was used together with a CCD camera. The objective was translated until the image being observed was in the objective's object plane.

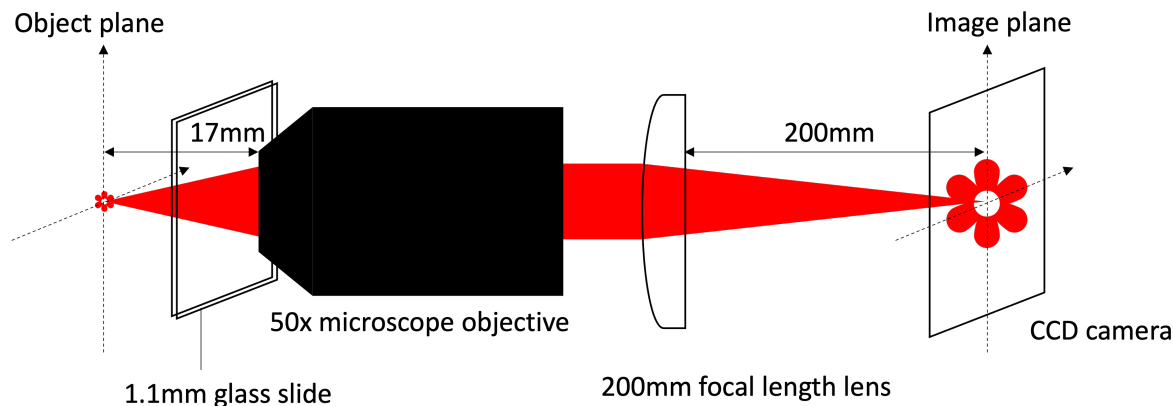


Figure 1: Diagram showing how a microscope objective was used to observe the images created

Because the objective was corrected for imaging through a 1.1mm glass slide, a microscope slide was placed in front of the objective. The objective was infinity corrected, and meant to be used with a 200mm focal length tube lens, so a 200mm focal length lens was placed behind the microscope objective. The distance between the tube lens and the microscope objective should be as close as possible to avoid vignetting.

Each square pixel on the CCD camera was $5.2\mu\text{m}$ in length. With the $50\times$ magnification of the microscope objective, one pixel on the CCD camera in the image plane of the objective corresponds to $0.104\mu\text{m}$ in the object plane of the objective.

3 Fiber mode field diameter measurements

3.1 Using the microscope objective to directly measure waist

To verify that measurements with the Mitutoyo gave accurate results, the fiber tip that the laser diode was coupled to was directly imaged with the Mitutoyo, using the setup shown Fig. 1, with the fiber tip in the objective's object plane. The fiber was specified to have a mode field diameter of $5.0 \pm 0.5\mu m$ [1].

In Mathematica, a 2D Gaussian fit was applied to the image using NonlinearModelFit with the fit function

$$I_0 \text{Exp} \left[-2 \left(\frac{(x - x_0)^2}{w_x^2} + \frac{(y - y_0)^2}{w_y^2} \right) \right] + \text{offset} \quad (1)$$

where I_0 is the amplitude, (x_0, y_0) are the coordinates of the center of the Gaussian, w_x^2, w_y^2 are the $1/e^2$ waists in the vertical and horizontal directions, and offset is a constant offset.

From the average of three separate measurements with the setup disassembled and reassembled in between, the fiber tip was observed to have a waist of

$$\begin{array}{c|c} w_x & w_y \\ \hline 2.60 \pm 0.05\mu m & 2.6 \pm 0.2\mu m \end{array}$$

Table 1: Measurement of fiber waist using the Mitutoyo microscope objective

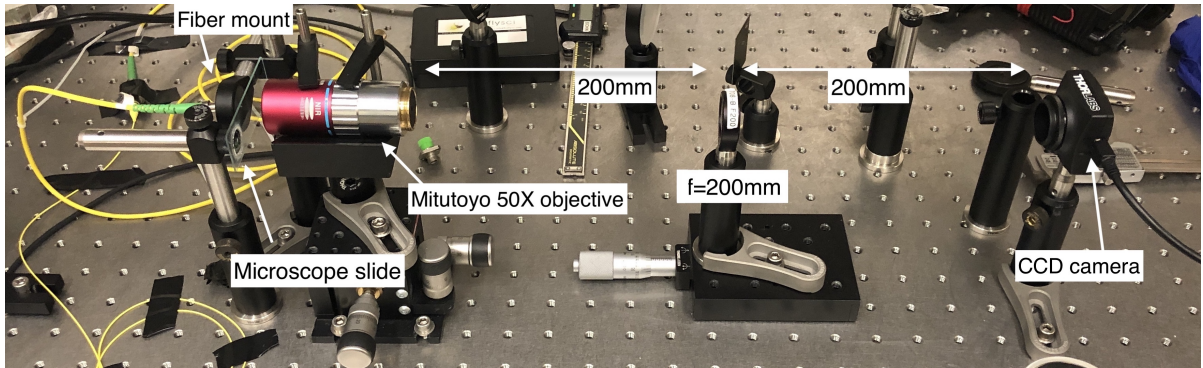


Figure 2: Setup for measurement of fiber mode field diameter using the Mitutoyo objective

This measurement was consistent with the expected value of $2.5 \pm 0.3\mu m$, so it was concluded that the microscope objective provided an accurate method to measure objects with features on the order of single microns.



Figure 3: Image of the fiber tip captured using the 50X microscope objective

3.2 Calculation of waist from beam divergence angle

The spot of a Gaussian beam has the following z-dependence [2]:

$$w(z) = w_0 \sqrt{1 + \frac{z^2}{z_R^2}}$$

where w_0 is the waist radius and z_R is the Rayleigh range, defined

$$z_R = \frac{\pi w_0^2}{\lambda}$$

and λ is the laser wavelength.

For $z \gg z_R$, the equation can be approximated by

$$\begin{aligned} w(z) &\approx w_0 \frac{z}{z_R} \\ &= \frac{\lambda}{\pi w_0} z \end{aligned} \tag{2}$$

Thus, one can make measurements of the beam's spot radius in the region $z \gg z_R$, where the beam has expanded to a size where it is easily measured, and then fit the measurements to Eq. 2 to find w_0 .

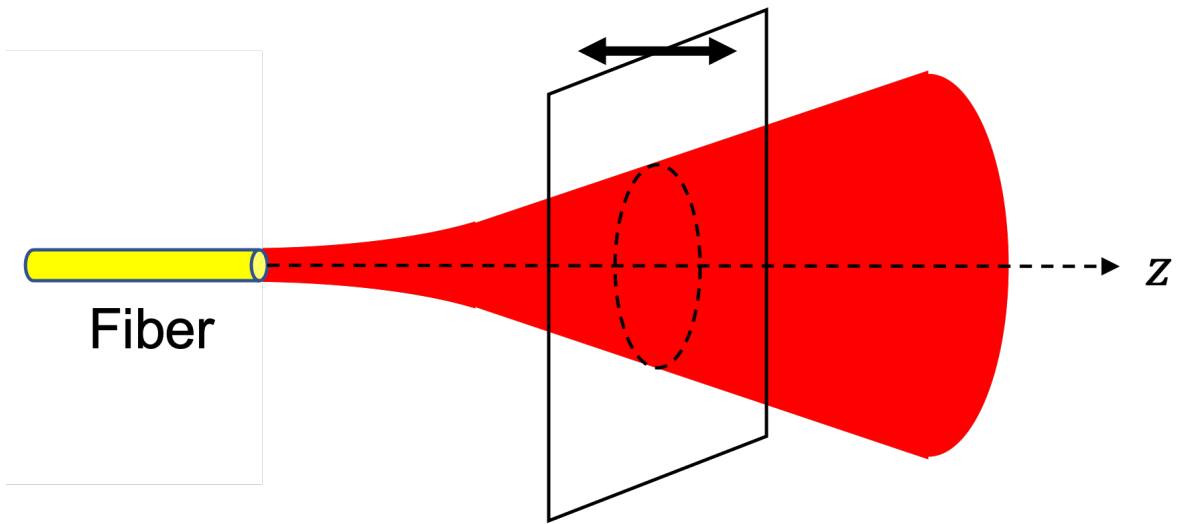


Figure 4: Measurements of the beam radius at different points along the z axis can be fitted to Eq. 2 to calculate w_0

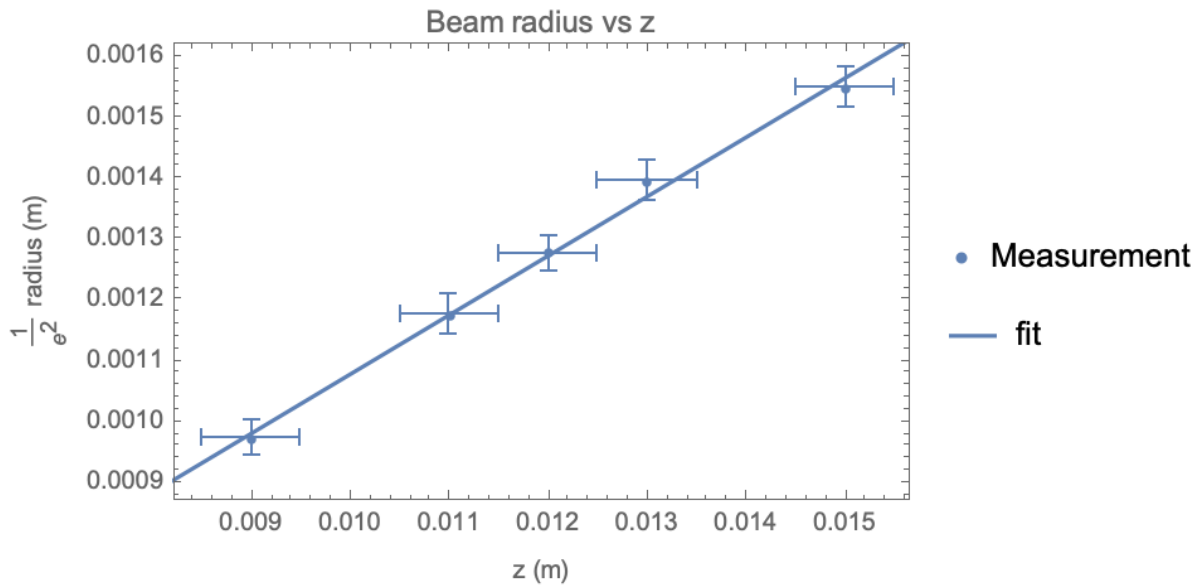


Figure 5: Beam radius measurements using the razor blade technique discussed in Sec. 3.2.1, fitted to Eq. 2 to find the fiber mode field diameter

The results from calculating the waist from the Gaussian beam equation and the waist measured with the Mitutoyo objective were consistent.

Method	w_0
Microscope	$2.60 \pm 0.05 \mu m$
Evolution	$2.59 \pm 0.21 \mu m$

Table 2: Comparison between the fiber mode field diameter measuring from measurement with the microscope objective and calculation from the Gaussian beam spot evolution equation (Eq. 2). Uncertainty was estimated by performing χ^2 fitting

3.2.1 Razor blade technique for measuring beam radius

To measure the beam radius at a given distance z , as shown in Fig. 4, the beam was shone onto a power meter and incrementally blocked by a razor blade on a translation stage moving in the x direction, and at distance z from the fiber tip, as shown in Figs. 6, 7.

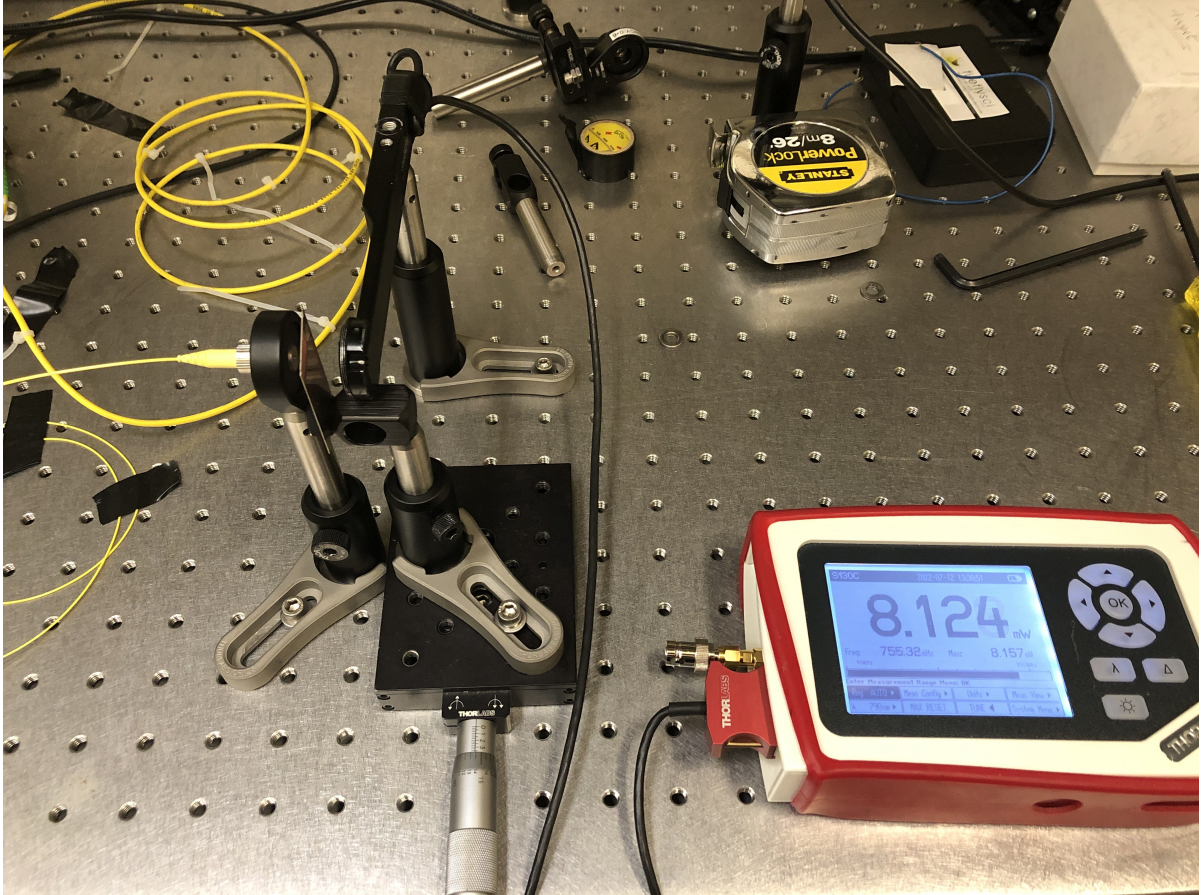


Figure 6: Setup used for taking razor blade measurements of beam radius, for calculating the mode field diameter of the optical fiber

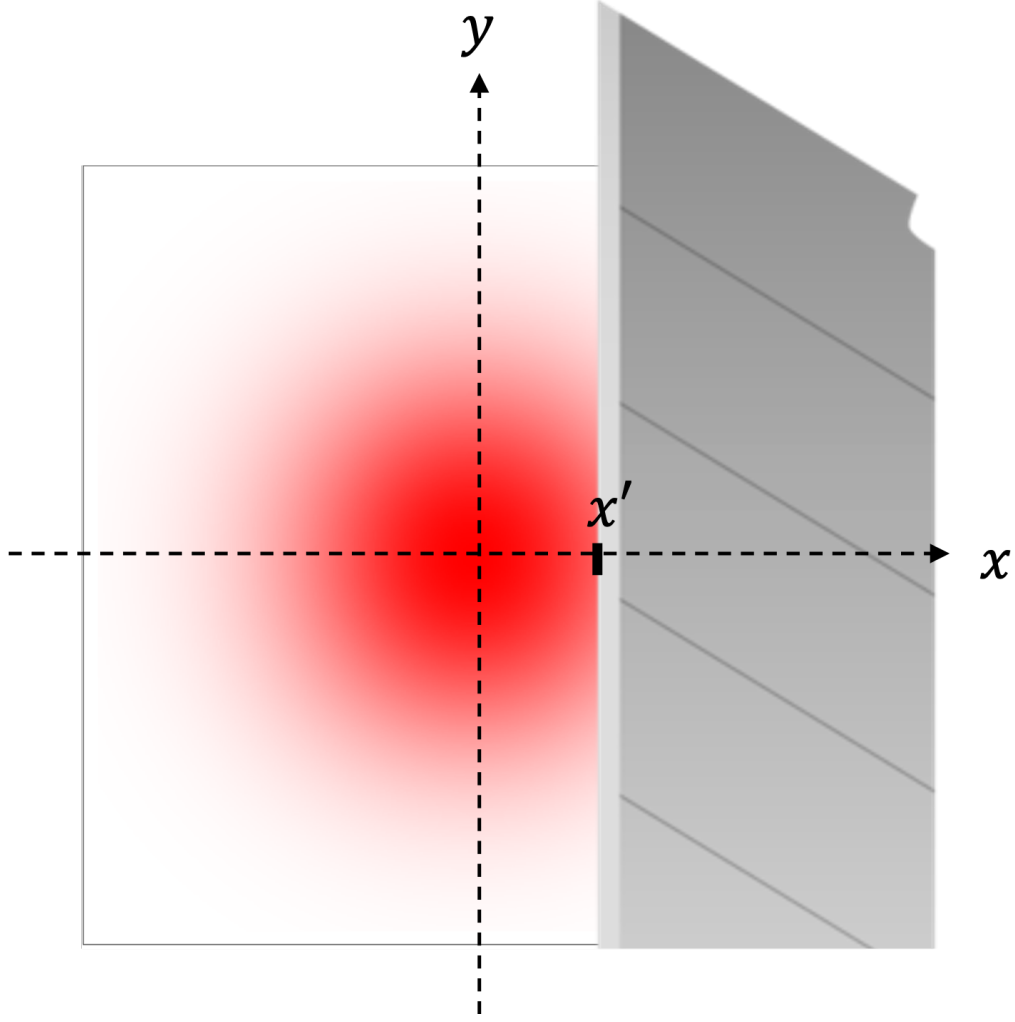


Figure 7: Razor blade edge at a distance x' along the x axis, blocking all light in the region $x > x'$

If we have an ideal Gaussian beam centered along the z axis, the total power transmitted by the beam through a given z plane without the razor blade there is the integral of the intensity over all space at that distance z

$$\int_{-\infty}^{\infty} \int_{-\infty}^{\infty} I_0 \text{Exp} \left[-2 \left(\frac{x^2 + y^2}{w(z)^2} \right) \right] dx dy$$

Of course, in reality, the powermeter cannot capture all of the beam's power in an infinite plane, but the fraction of the beam's power outside of its $1/e^2$ radius is $1/e^2$. If the powermeter's sensor area is twice as great as the beam's radius, it can capture over 99.9% of the total power.

Now, if the razor blade edge is perfectly straight and vertical, blocking all light at $x > x'$, the integral in the x direction only goes from $-\infty$ to x'

$$\begin{aligned} & \int_{-\infty}^{\infty} \int_{-\infty}^{x'} I_0 \text{Exp} \left[-2 \left(\frac{x^2 + y^2}{w(z)^2} \right) \right] dx dy \\ &= \int_{-\infty}^{\infty} I_0 e^{-2 \frac{y^2}{w(z)^2}} dy \int_{-\infty}^{x'} e^{-2 \frac{x^2}{w(z)^2}} dx \end{aligned}$$

For a given $w(z)$, the first integral can be evaluated to some constant. The second integral is a function of x' and can only be solved numerically, but it can be expressed in terms of error function

$$Erf(x') = \frac{2}{\sqrt{\pi}} \int_0^{x'} e^{-x^2} dx$$

We are only interested in the x' dependence, so let's lump all constants into a single constant C . Thus, the integral of power in the region not blocked by the razor blade becomes.

$$C(1 + Erf[\frac{\sqrt{2}x'}{w(z)}]) \quad (3)$$

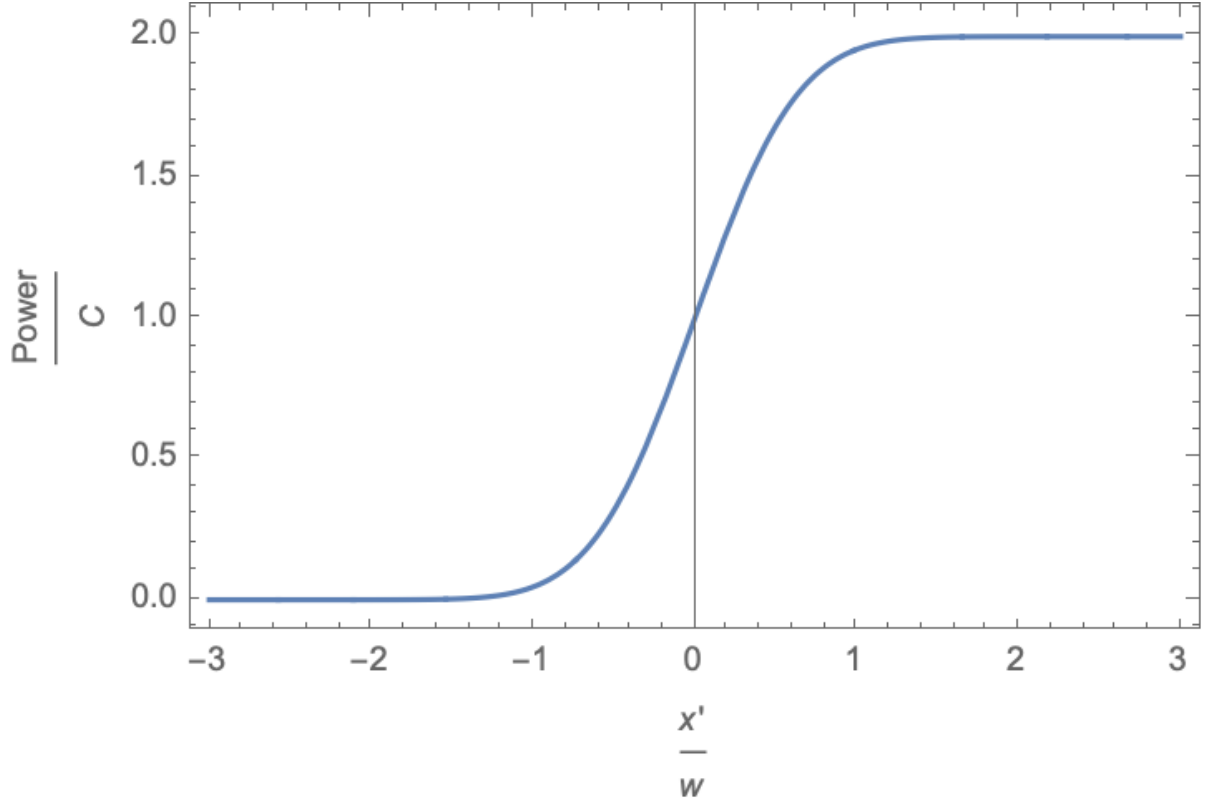


Figure 8: Plot of Eq. 3

The graph of Eq. 3 matches intuition, as the transmitted power remains roughly constant as the razor blade cuts into the beam from $+\infty$, changes rapidly as the razor blade crosses through the region for which $|x| < w(z)$, and then remains roughly at 0 as the razor edge approaches $-\infty$.

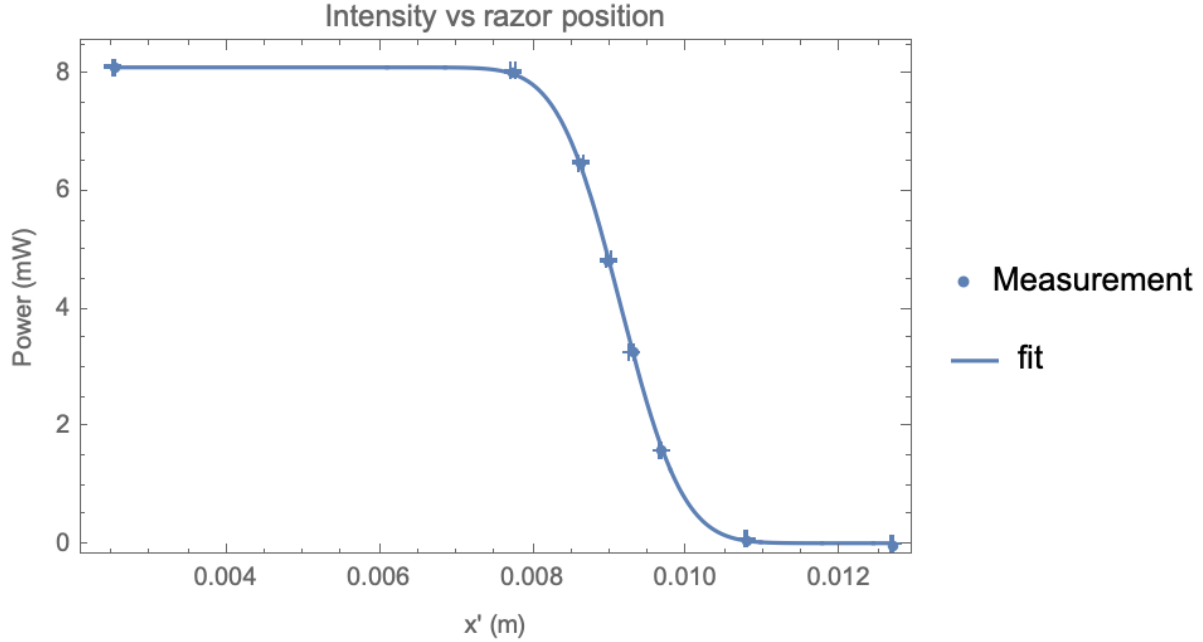


Figure 9: Example of a set of razor blade measurements fitted to the error function in Eq. 3 to determine $w(z)$, with x' replaced by $-x'$ to change the orientation of the error function

4 Choosing a focusing lens

The resolution of an optical system can be defined as the distance between the central maximum and first minimum of the airy disk created when focusing plane waves with the lens. This measure gives an idea of how sharp of an edge can be created. The equation for resolution is given below [3]:

$$\text{Resolution} = \frac{\lambda}{2NA} \quad (4)$$

where λ is the wavelength of light being used and NA is the numerical aperture. If our optical system is a single lens, we'd clearly want it to be a lens with large numerical aperture.



Figure 10: Photograph of the surroundings of the science cell, in which the BEC is manipulated

In Professor Schnelle's experimental setup, it is difficult to place a lens near the science cell inside which the BECs are held. The lens must be at least 40mm away from the BEC.

Initially, we wanted to use the Mitutoyo for focusing images onto the condensate. With its numerical aperture of 0.42, it would have a resolution limit of $0.94\mu m$. However, with its large size and 17mm working distance, it was too large to place close enough to the science cell to focus an image onto a condensate.

The two lenses that were tested for focusing an image onto BECs were the AL1815-B and AL2550-B from Thorlabs. Their specifications are given in the table below.

Lens	efl	NA	WD	Diameter
AL1815-B	15mm	0.53	11.5mm	18mm
AL2550-B	50mm	0.23	46mm	25mm

Table 3: Specifications for the Thorlabs AL1815-B and AL2550-B lenses, used in focusing images onto the BEC

The AL2550-B lens was chosen as it would fit in a mount designed by a previous graduate student, Joonhyuk Kwon. With a numerical aperture of 0.23, the expected resolution limit was

$$\text{Resolution} = \frac{790\text{nm}}{20.23} = 1.7\mu\text{m}$$

The AL1815-B lens would need to be mounted on a thin rod, as it would have to be inserted into the glass walls shown in Fig. 10

With a numerical aperture of 0.23, the expected resolution limit was

$$\text{Resolution} = \frac{790\text{nm}}{20.53} = 0.745\mu\text{m}$$

The resolution limit of the AL2550-B lens was over a factor of 2 larger than the AL1815-B, so it was expected that the AL2550-B would produce a sharper edge.

5 Choosing a collimating lens

Since the light used in imaging arbitrary potentials onto BECs is laser light, one must ensure that the wavefronts are collimated when they illuminate the object that is being imaged.

The laser diode used was the LPS-785-FC, which was pigtailed to 780HP fiber with a flat polished connector [4]. The mode field diameter of 780HP cable is $5\mu\text{m}$, which has a Rayleigh range of $25\mu\text{m}$ at 790nm. Thus, the beam diverges very quickly, necessitating a lens that collimated the beam coming out of the fiber.

The first collimator used was the CFC-11X-B from Thorlabs [5], as it was previously being used in Professor Schneble's setup. However, it produced a dark spot in the beam profile, and was thus not chosen for the final setup.

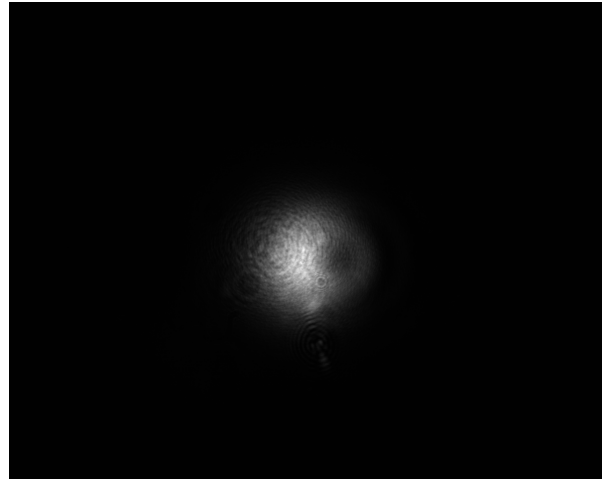


Figure 11: The CFC-11X-B adjustable collimator introduced a dark spot into the beam profile. Image produced by directly shining the collimated beam onto a CCD camera.

Second, the AL1815-B lens from Thorlabs was tested as a potential collimator [6]. However, this lens introduced a spiral pattern into the beam, and was thus not chosen for the final setup. The spiral pattern was likely a result of the polishing technique used in creating the lens. The presence of this pattern created doubt that the performance of the AL1815-B lens as an imaging lens would be better than the AL2550-B, but it proved to work well, as shown in Sec. 7.2.



Figure 12: The AL1815-B aspheric lens introduced a spiral pattern into the beam profile. Image produced by directly shining the collimated beam onto a CCD camera.

Third, the AL1225 lens from Thorlabs was used [7]. However, this lens created a bright ring in the edge of the beam, and when the beam was focused down, there was a dark spot in the center of the beam.

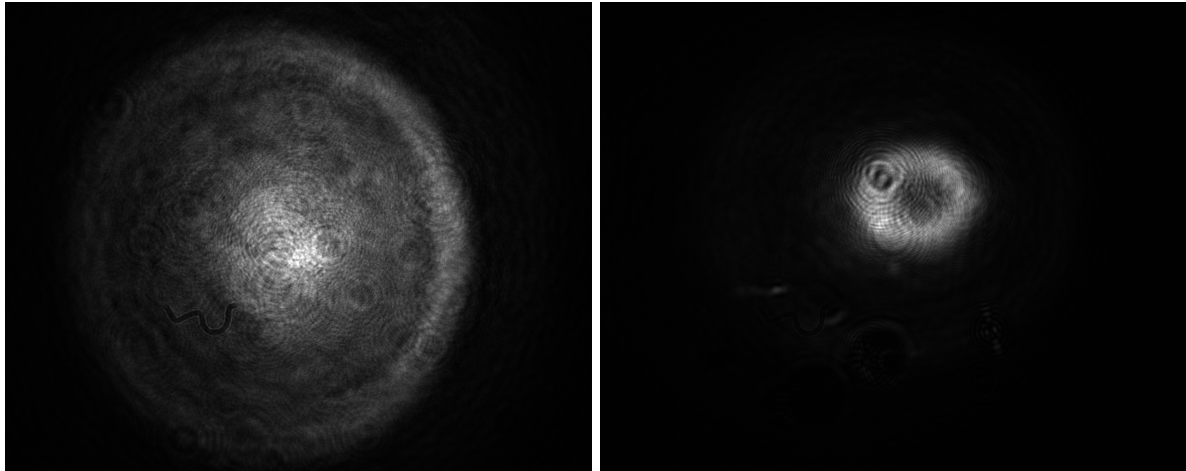


Figure 13: Beam collimated with the AL1225 lens had a bright ring around the edge (left). When the lens was placed so that it focused down the beam instead of collimating it, a dark ring became visible in the center of the beam (right). The beam was overfilling the lens

Lastly, the F230FC-B collimator was tested [8].

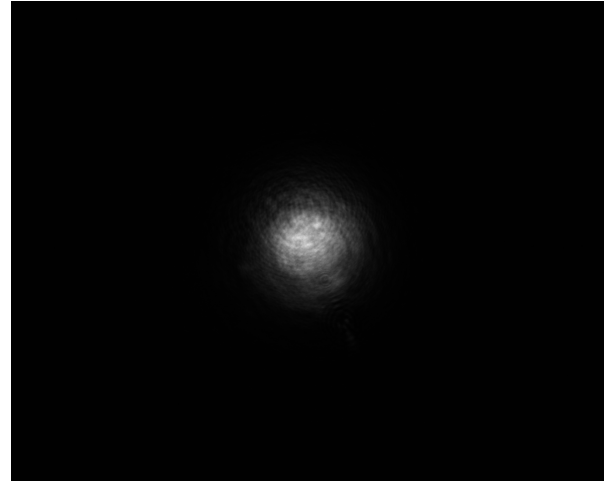


Figure 14: Image of the beam produced by the F230FC-B fiber collimator, captured after 100mm of propagation

It was concluded that it would be best to use the F230FC-B.

However, by measuring the beam profile with the CCD camera at three different locations along its propagation distance, it was shown that the beam wasn't collimated.

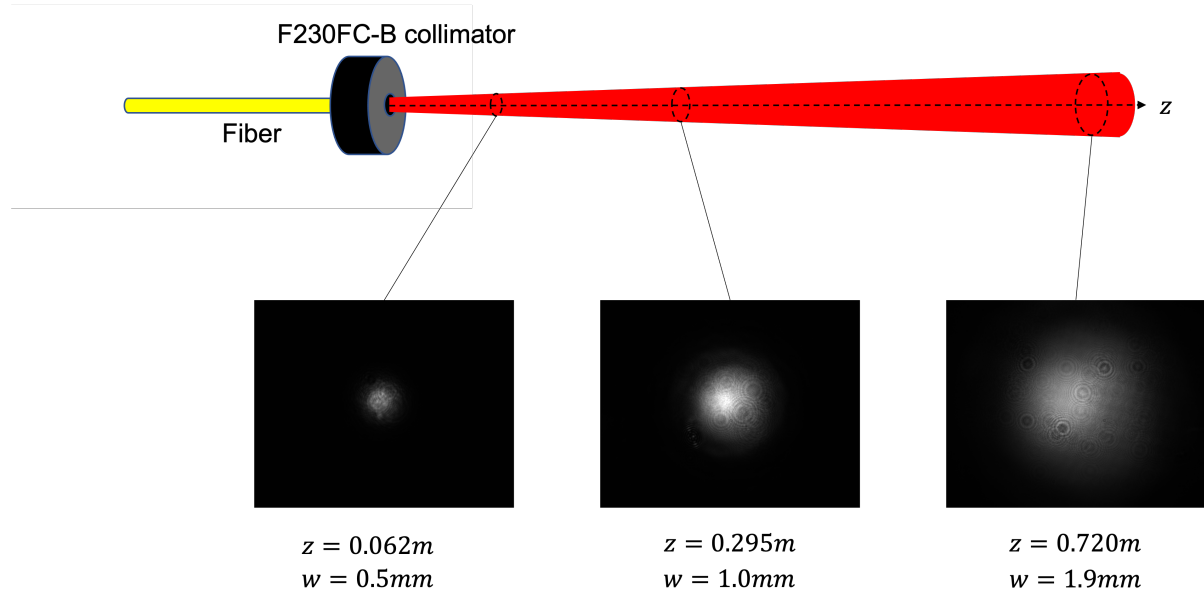


Figure 15: By measuring the beam profile with the CCD camera at three different locations along its propagation distance, it was shown that the beam was expanding. Each beam profile was fitted to a 2D Gaussian using Mathematica's NonlinearModelFit to determine the spot size, w

For a waist of 0.5mm, the Rayleigh range is

$$z_R = \frac{\pi(0.510^{-3}m)^2}{79010^{-9}m} \approx 1.0m$$

so the beam should only expand by a factor of $\sqrt{2}$ over 1m. As shown in Fig. 15, the beam was a factor of 2 larger at just 0.295m.

Even though the beam was still expanding after the F230FC-B collimator, it was still selected as part of the setup, as it is easier to work with a bigger beam.

6 Telescope for beam expansion

It was decided to build a telescope after the collimator to collimate the beam. The beam was also about a factor of 5 too small to fill the DMD's approximately $6 \times 10\text{mm}$ array, so the lenses were chosen to expand the beam waist to the proper size.

Lens	focal length
ACN127-030-B	-30mm
AC508-100-B	100mm

Table 4: Lenses chosen for the telescope used to collimate the beam after the fiber collimator

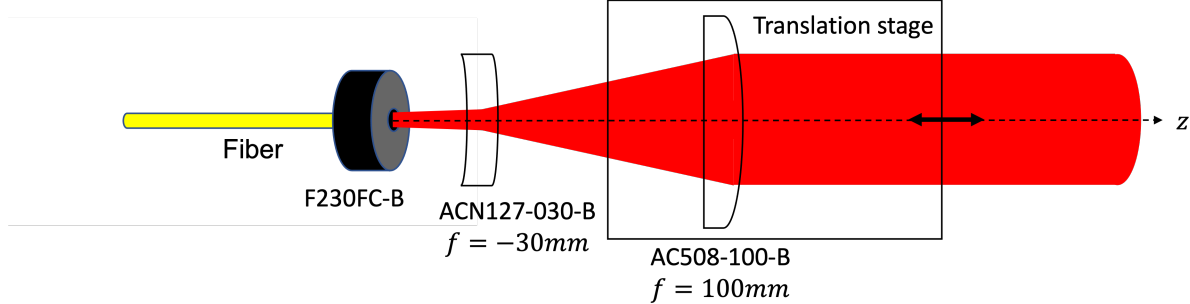


Figure 16: Positioning of telescope lenses used to collimate the beam after the fiber collimator. The AC508-100-B was placed on a translation stage so that its position could be finely adjusted.

The location of the AC508-100-B was adjusted with a translation stage until the beam no longer seemed to diverge by visual observation over the length of the room that the laser was in. The beam's divergence was again measured with a CCD camera as well.

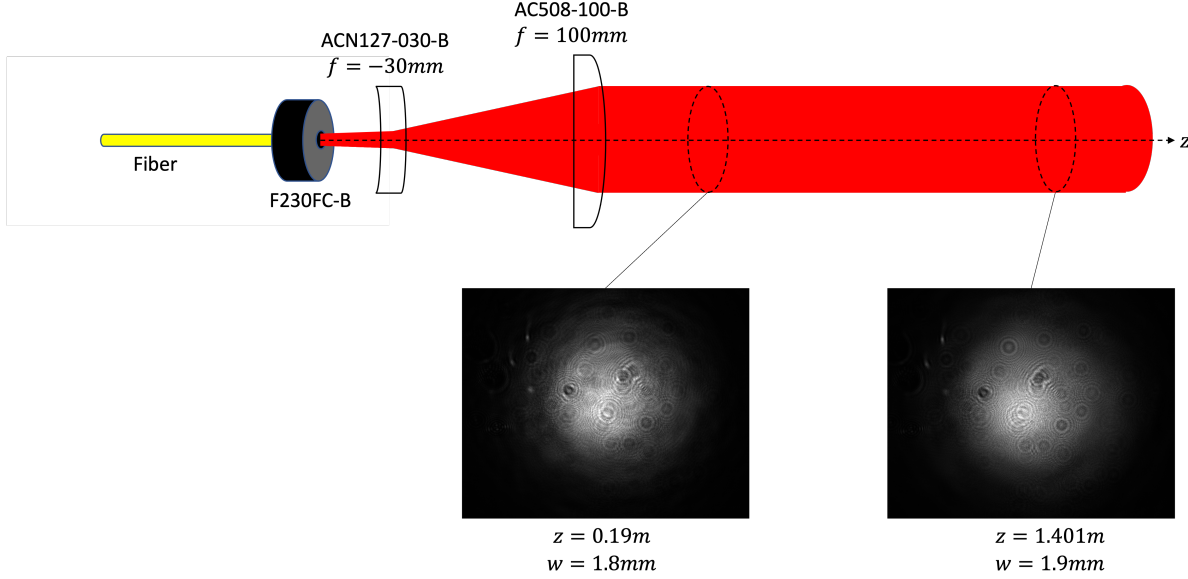


Figure 17: The beam profile was again measured with the CCD camera at two different locations along its propagation distance, and the beam was found to be collimated to a satisfactory degree. Each beam profile was fitted to a 2D Gaussian using Mathematica's NonlinearModelFit to determine the spot size, w

For a waist of 1.8mm , the Rayleigh range is approximately 13m , so the beam shouldn't expand much over 1m . Using ABCD matrices for Gaussian beam propagation, it was calculated that, for a beam perfectly collimated with a waist of 1.8mm , the beam should only increase by $5\mu\text{m}$. This means that the beam can be collimated better than was done for this experiment. Better collimation should be achieved if this experiment were to be done again.

7 Imaging an edge

The DMD is acts as an amplitude mask, meaning that it blocks parts of the outgoing beam. Instead of using a DMD to image an edge, as the DMD is a reflective device and thus complicates the geometry of the setup, a 1951 USAF target was used, as it is an amplitude mask which includes very sharp edges.

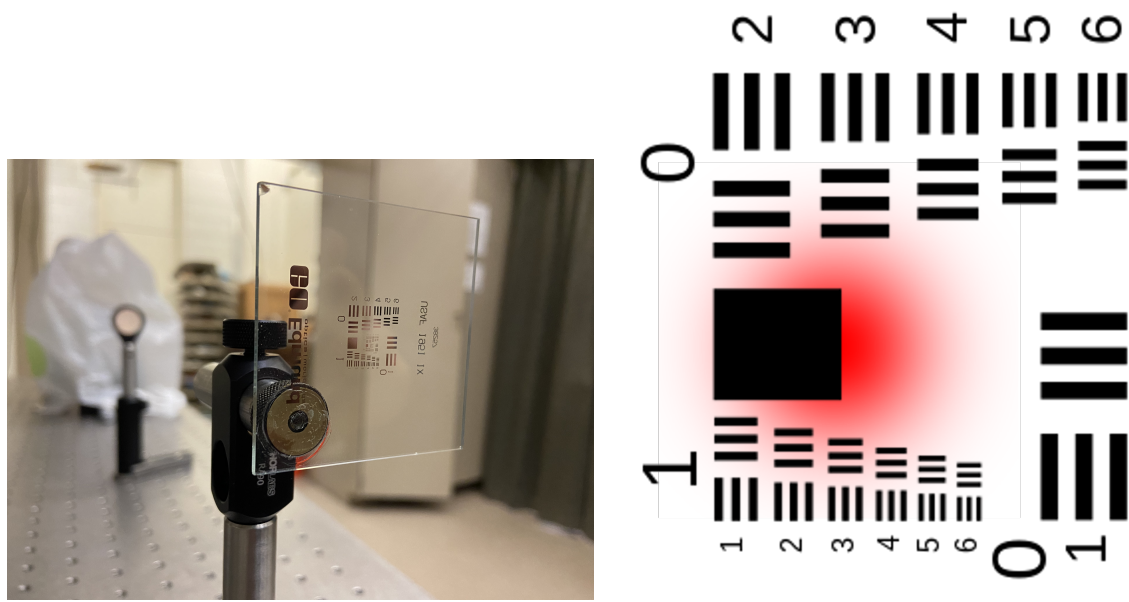


Figure 18: The air force target is a glass plate with a reflective pattern printed on one side (left). A solid square in the pattern was selected for use as an edge to image (right)

7.1 Single lens

Initially, a setup was designed with a single lens for focusing.

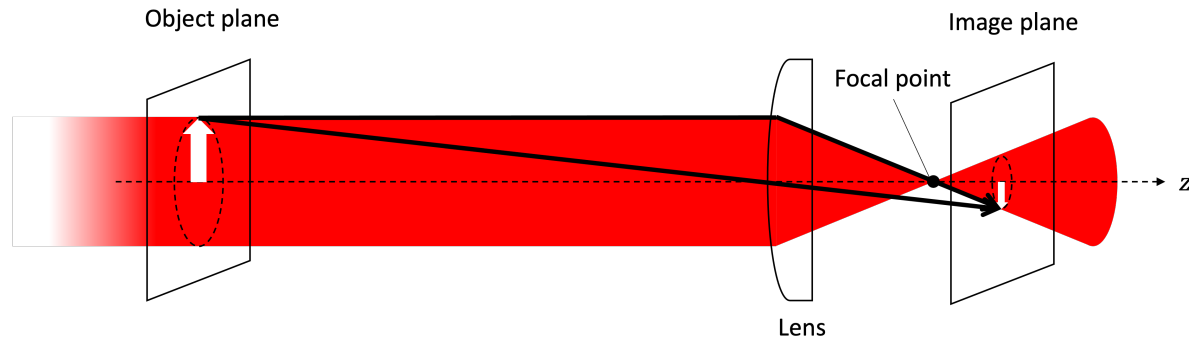


Figure 19: Diagram showing how a single lens can be used to focus an image in a given object plane onto the corresponding image plane. The illuminating beam's evolution is shown in red. The rays used to determine the image position are shown as black arrows

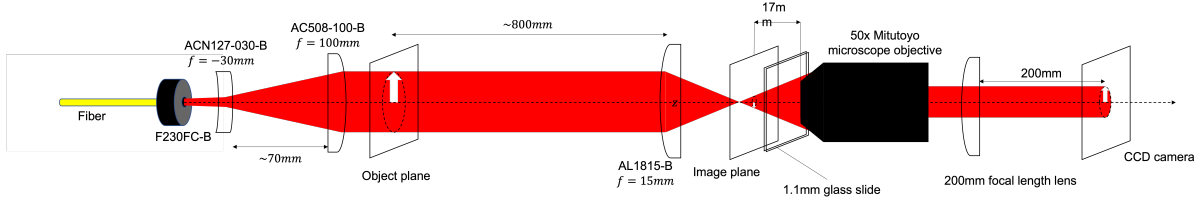


Figure 20: Diagram of the full setup used for imaging with a single lens, including the Mitutoyo microscope objective used to observe the image being formed

Initially, the AL2550-B lens was used instead of the AL1815-B, but it did not provide the desired sharpness. The edge rose over a distance of about $10\mu\text{m}$, as seen in Fig. 21.

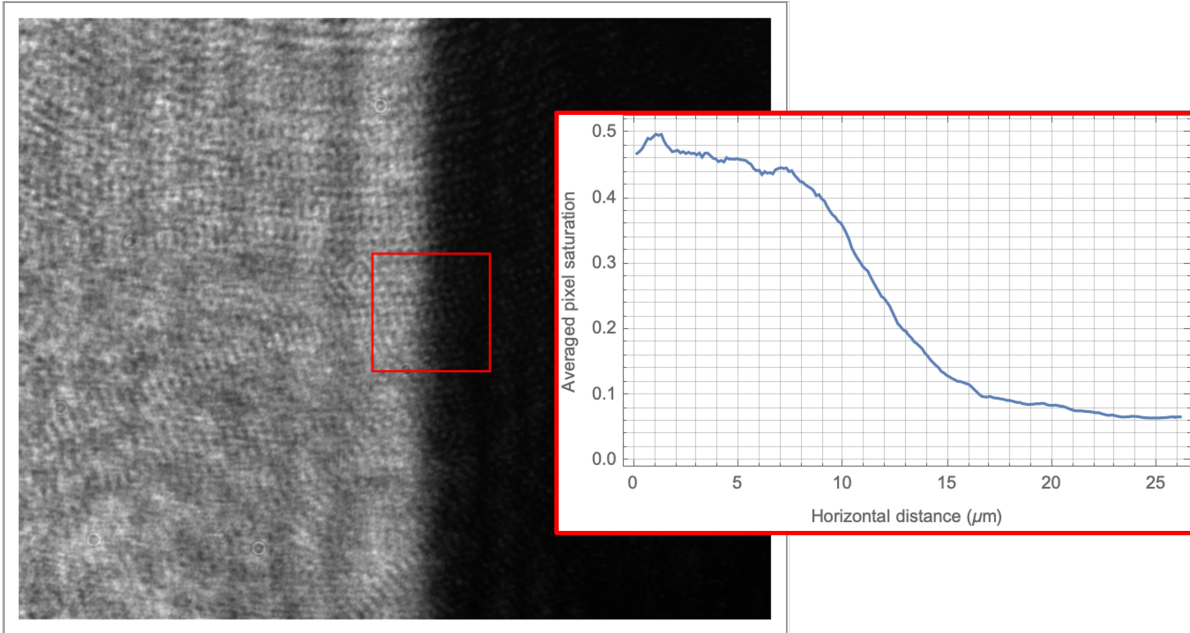


Figure 21: Image of the edge produced by the setup in Fig. 20, but with the AL2550-B lens instead of the AL1815-B. The intensity values within the 200×200 pixel red square in the image were selected for analysis. The intensity values for each column were averaged, and each column was assigned its corresponding distance in the focus of the Mitutoyo.

Thus, the AL1815-B lens was chosen to be the focusing lens over the AL2550-B lens. The edge produced by the AL1815-B lens rose over a distance of about $2\mu\text{m}$, as seen in Fig. 22.

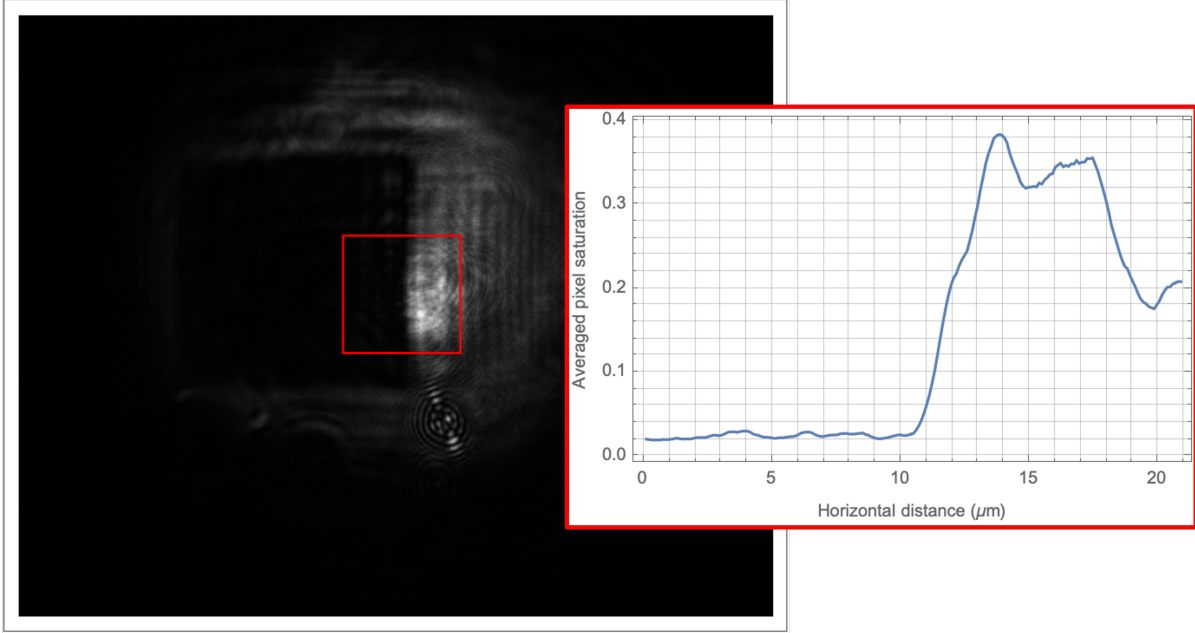


Figure 22: Image of the edge produced with the setup shown in Fig. 20. The intensity values within the 200×200 pixel red square in the image were selected for analysis. The intensity values for each column were averaged, and each column was assigned its corresponding distance in the focus of the Mitutoyo.

As seen in Fig. 22, there is significant distortion warping the edges of the square. Thus, a second setup was designed and tested.

7.2 Two lenses

7.2.1 Setup

After imaging with a single lens, a system with two lenses was devised. The system was designed so that the beam would pass through the image plane collimated if no object was present, and so that the object and image were each located one focal length from their nearest lens.

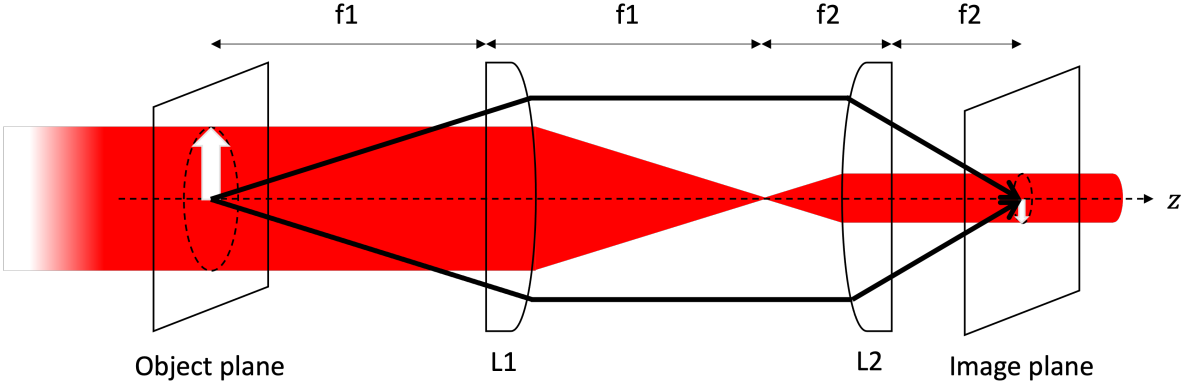


Figure 23: Diagram showing the setup used for imaging with two lenses. An object in the focal plane of a lens L_1 with focal length f_1 becomes focused in the focal plane of lens L_2 with focal length f_2

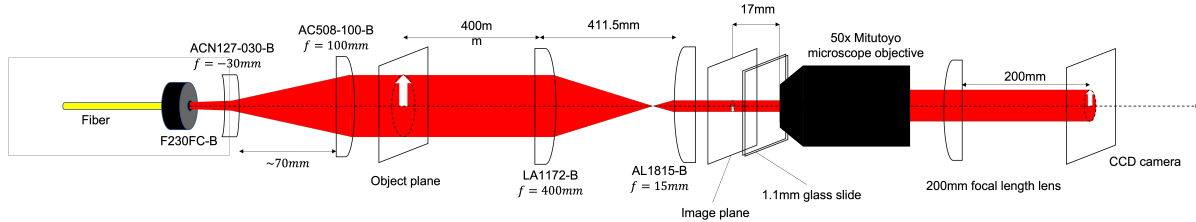


Figure 24: Diagram of the full setup used for imaging with two lenses

7.2.2 Results

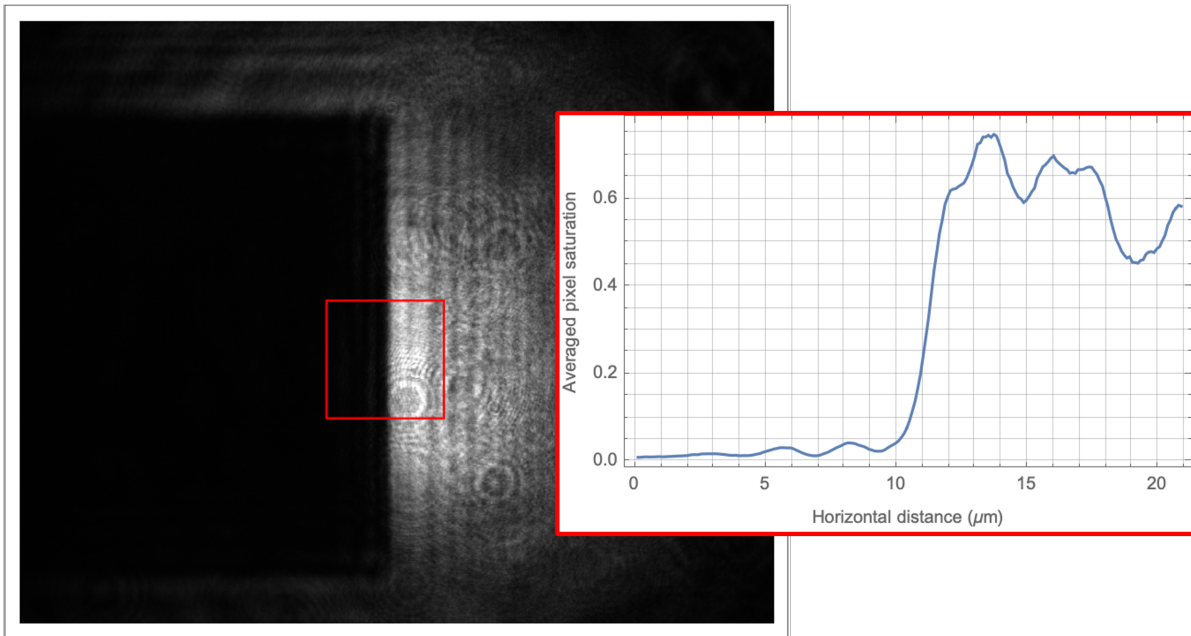


Figure 25: Image of the edge produced with the setup shown in Fig. 24. The intensity values within the 200×200 pixel red square in the image were selected for analysis. The intensity values for each column were averaged, and each column was assigned its corresponding distance in the focus of the Mitutoyo.

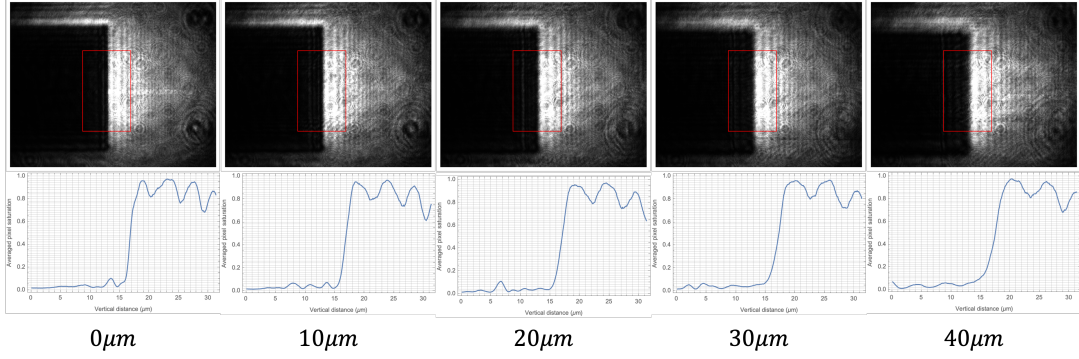


Figure 26: Edge profile over varying distance around the best focus. Between the different measurements in each column, the Mitutoyo's position was incremented by $10\mu m$ along the z axis of Fig. 24. The intensity values within the 200×200 pixel red square in the image were selected for analysis. The intensity values for each column were averaged, and each column was assigned its corresponding distance in the focus of the Mitutoyo.

The edge took about $2\mu m$ along the horizontal direction to go from its lower level to its upper level, similar to the result with the single lens shown in Fig. 22. However, the result with two lenses showed significantly less distortion of the edge.

The edge width is still about $3\times$ its theoretical limit, so further work is necessary to approach this limit.

7.2.3 Beam size

The size of the beam before and after passing through the setup shown in Fig. 23 was measured in order to compare its evolution to theoretical calculation, to verify that the setup is functioning as expected.

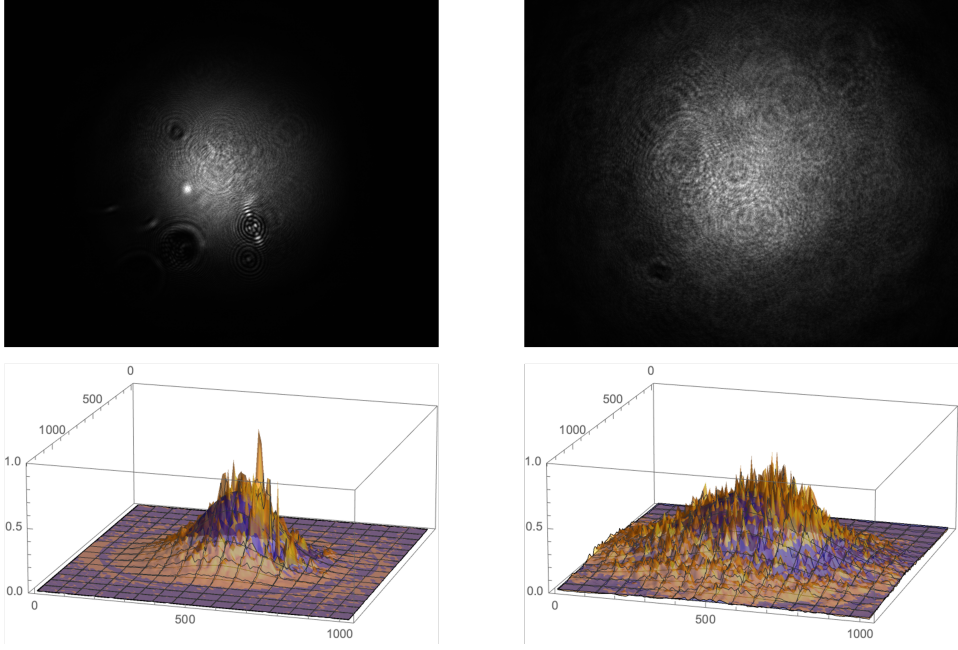


Figure 27: Size of the beam at the object (left) and image (right) planes of Fig. 24, captured on the CCD camera and fitted to a 2D Gaussian distribution in Mathematica. The bottom row shows the comparison between the raw data in orange and the fit in blue for both beams. The beam on the right was observed using the Mitutoyo objective, and thus was magnified 50 \times .

	w_x	w_y
Initial beam	1.3mm	1.3mm
Final beam	55 μm	56 μm

Table 5: w_x, w_y are the horizontal and vertical radii of the fitted 2D Gaussian for the initial and final beams

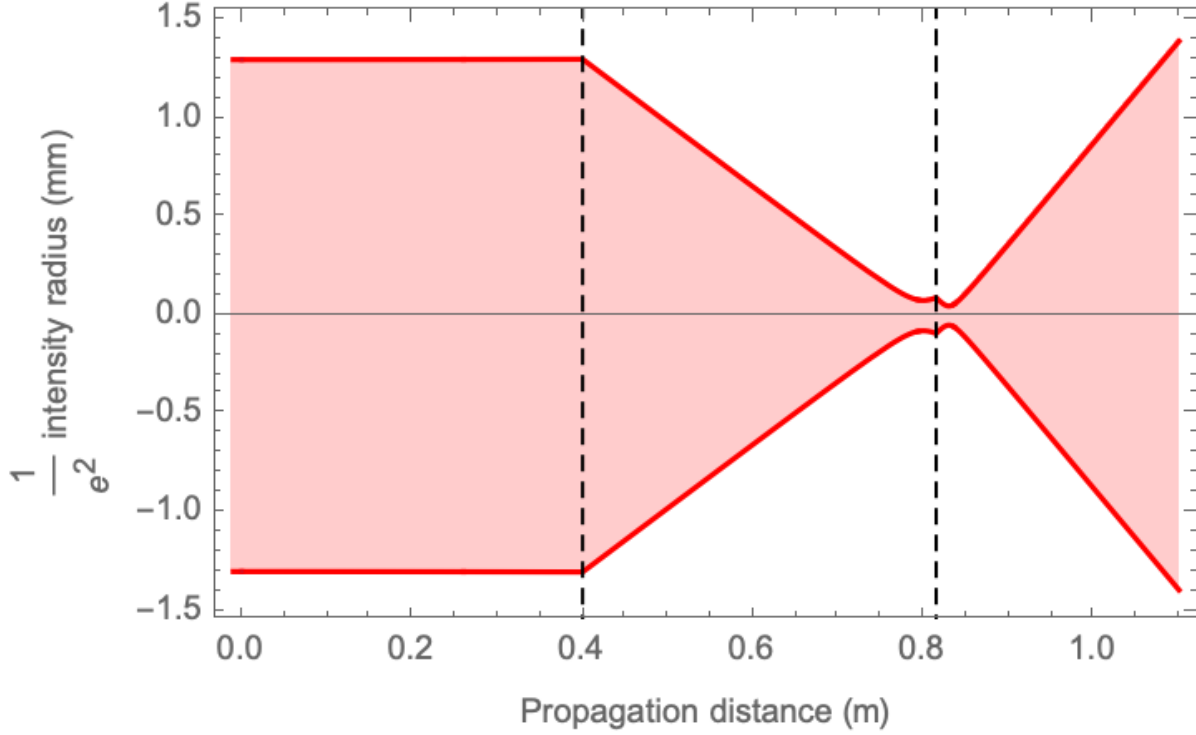


Figure 28: Using ray matrices [9], the evolution of a Gaussian beam through the optical system shown in Fig. 23 was calculated. The left dashed line indicates the location of the 400mm focal length LA1172-B lens, and the right dashed line indicates the location of the 15mm focal length AL1815-B lens.

Measured	Expected
$55\mu m$	$49\mu m$

Table 6: Measured and expected beam waist in the image plane given after the measured initial beam passes through the optical system in Fig. 23

The final beam's size was within 11% of the expected value calculated with ray matrices. As the measured and expected beams were of the same order of magnitude, it was concluded that the optical system was functioning as expected.

7.2.4 Image demagnification

The 1951 USAF air force target has different sets of lines with known spacings. By imaging the target, one can determine the magnification of the optical system and the smallest resolvable feature size for any given object.

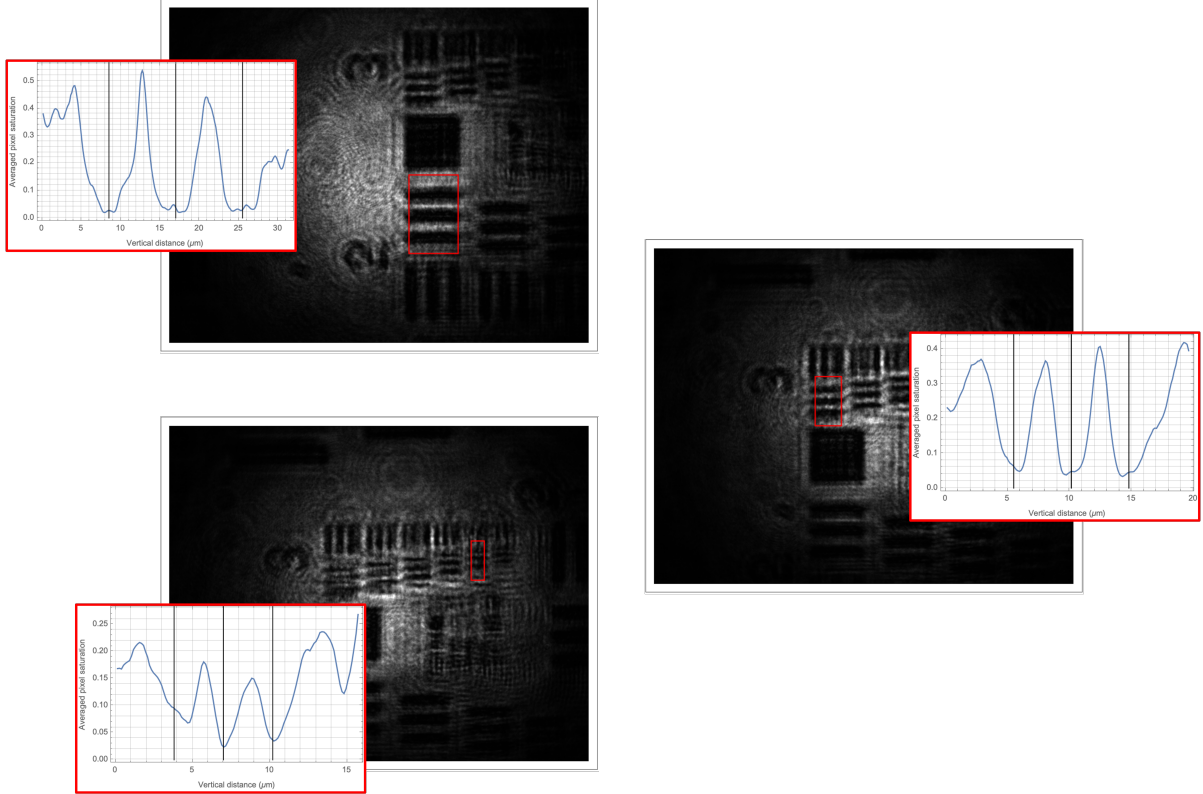


Figure 29: Different sets of lines with known spacings were imaged to calculate the optical system’s magnification of the object. The intensity values within the 200×200 pixel red square in each image were selected for analysis. The intensity values for each column were averaged, and each column was assigned its corresponding distance in the focus of the Mitutoyo.

Group, Element	Actual dist/line	Measured dist/line	Magnification (\times)
2,1	$250\mu m$	$(8.5 \pm 0.5)\mu m$	29 ± 2
3,1	$125\mu m$	$(4.5 \pm 0.5)\mu m$	28 ± 2
3,5	$79\mu m$	$(3.2 \pm 0.5)\mu m$	25 ± 2

Table 7: Spacings for different elements on the 1951 USAF resolution target [10], their size in the image of the air force target, and the resulting calculated magnification

It is unclear why the calculated demagnification was inconsistent for different elements on the resolution target. This inconsistency indicates that a better method for determining the line pairs per meter must be devised, as it was estimated by hand.

The expected demagnification was calculated from the ratio of the focal lengths of the *LA1172 – B* and *AL1815 – B* lenses to be $400/15 = 27$. All of the measured values of the magnification were consistent with $27\times$.

The smallest resolvable feature seems to be the element (3,5), which has a feature size of $79\mu m$ at the object and $3.2\mu m$ at the image. For $5.4\mu m$ mirror size on the DMD, $79\mu m$ corresponds to 15 micromirrors on the DMD. Thus, unless the optical system resolution can be improved, any features created on the DMD must about 15 micromirrors or larger in order to be resolvable.

8 Conclusions

The AL2550-B lens had resolution an order of magnitude worse than the AL1815-B, and thus was not chosen as a focusing lens.

The best resolution was achieved using a setup with two lenses: the AL1815-B and the LA1172 lens. An edge sharpness was achieved of about $2\mu m$, and it was shown to stay at about 2μ over a distance of $50\mu m$ along the beam's direction of propagation.

The optical system was shown to demagnify the object by about $27\times$. While a $2\mu m$ edge was achieved, the smallest resolvable pattern on the USAF target was $3.2\mu m$ at the image and $79\mu m$ at the object, corresponding to about 15 micromirrors. Thus, it was concluded that patterns on the DMD must have features with sizes greater than 15 micromirrors in order to be resolvable.

With the BEC sitting in a lattice with a spacing of about $790nm/2 = 345nm$, the $2\mu m$ edge would rise over about 6 lattice sites. The AL1815-B's theoretical resolution limit of $745nm$ has not yet been achieved, and would be a significant improvement on current results.

References

- [1] Thorlabs. 780hp single mode fiber. [Online]. Available: <https://www.thorlabs.com/thorproduct.cfm?partnumber=780HP>
- [2] E. J. Galvez, “Gaussian beams,” 2014. [Online]. Available: <https://www.colgate.edu/media/5371/download>
- [3] R. Rottenfusser. Numerical aperture and resolution. [Online]. Available: <https://zeiss-campus.magnet.fsu.edu/articles/basics/resolution.html>
- [4] Thorlabs. Sm fiber-pigtailed laser diode. [Online]. Available: <https://www.thorlabs.com/thorproduct.cfm?partnumber=LPS-785-FC>
- [5] ——. Adjustable fc/pc collimator. [Online]. Available: <https://www.thorlabs.com/thorproduct.cfm?partnumber=CFC-11X-B>
- [6] ——. Aspheric lens. [Online]. Available: <https://www.thorlabs.com/thorproduct.cfm?partnumber=AL1815-B>
- [7] ——. Aspheric lens. [Online]. Available: <https://www.thorlabs.com/thorproduct.cfm?partnumber=AL1225>
- [8] ——. Aspheric lens. [Online]. Available: <https://www.thorlabs.com/thorproduct.cfm?partnumber=F230FC-B>
- [9] G. Fowles, *Introduction to Modern Optics*, ser. Dover Books on Physics. Dover Publications, 2012. [Online]. Available: <https://books.google.com/books?id=VeS7AQAAQBAJ>
- [10] E. Optics. 1951 usaf resolution calculator. [Online]. Available: <https://www.edmundoptics.com/knowledge-center/tech-tools/1951-usaf-resolution/>